IJARCCE ISSN (O) 2278-1021, ISSN (P) 2319-5940

International Journal of Advanced Research in Computer and Communication Engineering

Impact Factor 8.102 ⁜ Peer-reviewed & Refereed journal ⁜ Vol. 14, Issue 1, January 2025

DOI: 10.17148/IJARCCE.2025.14127

Design and Optimization of a Dual-Core Gold-Coated PCF-SPR Biosensor for Biosensing Applications

M. R. Khatun [1], M.S. Islam [2], Mithila Akter[3], Umme Salma[4], Afsana Islam [5]

Assistant Professor, Department of Computer Science and Engineering, Bangladesh University, Dhaka, Bangladesh[1]

Professor, Institute of Information and Communication Technology (IICT),

Bangladesh University of Engineering and Technology (BUET), Dhaka, Bangladesh[2]

Student, Department of Computer Science and Engineering, Bangladesh University, Dhaka, Bangladesh[3]

Assistant Professor, Department of Computer Science and Engineering, Bangladesh University, Dhaka, Bangladesh[4]

Senior Lecturer, Department of Computer Science and Engineering, Bangladesh University, Dhaka, Bangladesh[5]

Abstract: Photonic Crystal Fiber based Surface Plasmon Resonance (PCF-SPR) is a biosensing technology that combines PCF and SPR to detect refractive index (RI) changes with high sensitivity. This study investigates a novel dual-core PCF-SPR biosensor, designed to cover the RI range of 1.31 to 1.40, enhancing sensitivity and resolution for high-performance biosensing applications. It also focusing on key performance metrics, including wavelength sensitivity (WS), amplitude sensitivity (AS), and figure of merit (FOM), while minimizing confinement loss (CL). The methodology employs COMSOL Multiphysics using the Finite Element Method (FEM) for numerical analysis, investigating the effects of geometrical parameters on CL, AS, and WS. The results demonstrate a maximum WS of 8000 nm/RIU, an AS of -1279.38 1/RIU, a competitive resolution of 1.25×10^{-5} RIU, and an impressive FOM of 250 RIU^{-1}, which significantly outperform previous models. This biosensor presents an innovative and effective solution for biosensing applications, providing exceptional performance in the target RI range and demonstrating a strong potential for practical use in medical diagnostics and other biosensing fields.

Keywords: Photonic Crystal Fiber (PCF), Surface Plasmon Resonance (SPR), Biosensing, Finite Element Method (FEM), Confinement Loss (CL), Wavelength Sensitivity (WS), Figure of Merit (FOM).

I. INTRODUCTION

Photonic crystal fiber (PCF), first introduced by Knight et al. in 1996, is an advanced optical biosensing technology that utilizes specialized fibers to detect refractive index (RI) changes caused by molecular interactions. Unlike traditional optical fibers, PCFs are designed with a periodic arrangement of microscopic air holes along their length, which can guide light through mechanisms such as modified total internal reflection or photonic bandgap guidance [1]. In the past decade, remarkable progress has been achieved in enhancing these properties for a wide range of sensing applications. Notably, the outstanding sensitivity of PCF has been highly effective in overcoming challenges related to surface plasmon resonance (SPR)-based sensing. The performance of biosensors, particularly their sensitivity, is highly influenced by the choice of materials and design configurations [2]. To enhance the performance of PCF-SPR biosensors, reducing confinement loss is a critical in design consideration. Recent advancements in PCF-SPR biosensors have demonstrated remarkable sensitivity and specificity. These biosensors are widely employed in applications such as medical diagnostics, biochemical research, bioorganic sample analysis, and clinical testing [3] [4].

Current advancements in this domain have unlocked new opportunities for the application of PCF-SPR biosensors, signifying a transformative progression in their functionality and potential. For instance, the study [5] investigated the effect of varying the lattice pitch and the number of cladding rings on the confinement loss of PCF-SPR biosensors, revealing the influence of these parameters on sensor performance. Another study [6] modeled a five-ring hexagonal photonic crystal fiber using OptiFDTD 8 simulation software to explore the challenges of confinement loss and dispersion in PCF. To optimize the sensing capabilities of PCF-SPR, researchers have proposed incorporating plasmonic metal layers around the fiber surface or air holes [7] [8]. This modification enables the coupling of surface plasmon polariton (SPP) with core modes, improving sensing performance.

DOI: 10.17148/IJARCCE.2025.14127

SPR technology encompasses diverse sensing mechanisms, with external and internal sensing modes explored in several studies [9] [10] [11]. Various geometric parameters, such as analyte layer thickness, gold layer thickness, perfectly matched layer (PML) thickness, and the radius and spacing of air holes, have been adjusted to achieve the desired performance levels [12]. Contemporary research has focused on the high sensitivity, compact structure, and versatility of PCF-based SPR sensors, leading to significant improvements in performance and expanded application areas [13] [14]. Notably, an indium tin oxide (ITO) layer with a thickness of 110 nm enabled a high wavelength sensitivity (WS) [15]. One study introduced a birefringent PCF-SPR biosensor with side polishing, showing that applying a side coating on a flat ITO surface improved plasmon excitation when interacting with an analyte. Similarly, another study [16] designed a PCF sensor featuring an oxidation-resistant silver layer, where the birefringent structure enhanced sensitivity in the core-guided mode. These works highlight various design strategies for optimizing PCF-SPR sensor performance.

Previous research indicate that the properties of PCF-SPR biosensors can be effectively tailored by adjusting design parameters and selecting appropriate coating materials. These investigations contribute to the ongoing development of PCF-SPR biosensors, addressing existing challenges, refining designs, and offering valuable insights into improving sensitivity and specificity. Despite significant progress, confinement loss (CL) remains a major obstacle, as it reduces sensor sensitivity and limits the ability to detect analytes. Researchers have explored several approaches to address this challenge, including experimenting with alternative materials and refining geometric designs. However, there remains a clear gap in the development of SPR biosensors that combine low confinement loss, high sensitivity, and simple fabrication processes. Addressing these limitations could unlock the full potential of PCF-SPR biosensors, transforming them into even more practical tools for a wide range of applications.

This study introduces a novel dual-core PCF-SPR biosensor designed to maintain consistent performance despite potential manufacturing challenges. The proposed model focuses on optimizing key performance metrics, including CL, WS, amplitude sensitivity (AS), and figure of merit (FOM). The primary objectives are as follows:

- Develop an innovative dual-core PCF-SPR biosensor.
- Refine the SPR model's geometry to achieve optimal performance outcomes.
- Ensure minimal confinement loss while significantly enhancing amplitude and wavelength sensitivity, as well as better resolution, across a broad RI range of 1.31 to 1.40, utilizing gold as the plasmonic material.

II. MATERIALS AND METHODS

The workflow involves designing a dual-core PCF-SPR biosensor and creating a mesh model in COMSOL Multiphysics to identify core and surface plasmon polariton (SPP) modes and evaluate the effective refractive index (N_{eff}) Numerical calculations are performed to determine key performance metrics, including confinement loss (CL), absorption sensitivity (AS), wavelength sensitivity (WS), and figure of merit (FOM).

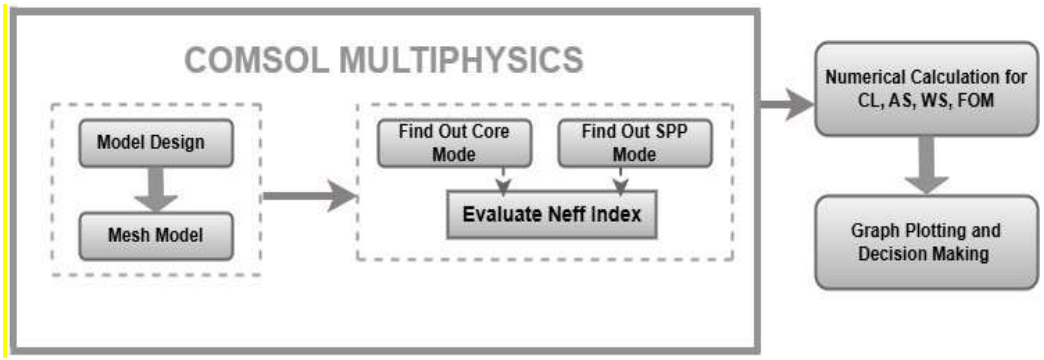

Figure 1. Workflow of the research procedure.

The design optimizes layers of gold, fused silica, air, and analyte by varying geometric parameters such as the gold layer thickness t_g, air hole diameters (d1 and d2), pitch , and perfectly matched layer (PML). Larger air hole diameters (d1) enhance core light confinement but risk increased scattering losses, while smaller diameters (d2) reduce scattering at the cost of weaker confinement. The pitch governs light confinement, with smaller values reducing leakage but

IJARCCE ISSN (O) 2278-1021, ISSN (P) 2319-5940

International Journal of Advanced Research in Computer and Communication Engineering

Impact Factor 8.102 ⁜ Peer-reviewed & Refereed journal ⁜ Vol. 14, Issue 1, January 2025

DOI: 10.17148/IJARCCE.2025.14127

potentially impeding propagation. Optimizing t_g balances sensitivity and light absorption to minimize CL. Using photonic bandgap engineering and PML further reduces leakage, achieving high sensitivity, minimal confinement loss, and effective signal quality in the biosensor.

Table 1 provides the numerical values of geometry parameters and materials used in the proposed PCF-SPR biosensor. The optimized design ensures high sensitivity and resolution for refractive index sensing applications. The detailed configurations of the SPR model components are summarized below:

TABLE I NUMERICAL VALUES OF GEOMETRY PARAMETERS AND MATERIALS USED IN PROPOSED PCF-SPR BIOSENSOR

Description of Parameters	Value	Unit
Smaller air hole (d1)	0.6	µm
Larger air hole (d2)	1	µm
Pitch (p)	2	µm
Thickness of gold (t_g)	40	nm
Fused silica layer (R1)	2.4*p	µm
Analyte outer layer (R2)	2.8*p	µm
PML outer layer (R3)	3.2*p	µm

The proposed PCF-SPR biosensor features a dual air-hole structure with smaller air holes d1=0.6 µm and larger air holes d2=1 µm, arranged in a periodic lattice with a pitch of p=2 µm. The fused silica layer, ensuring structural stability, has a radius of R1 = 4.8 µm while the analyte layer, designed for efficient interaction, has an outer radius of R2 = 5.6 µm and a thickness of 0.76 µm. To enhance the SPR effect, the design incorporates a 40 nm-thick gold layer t_g = 40 nm. A PML with a radius of R3 = 6.4 µm = 6.4, and a thickness of 0.8 µm minimizes reflection losses. Optimized for refractive index sensing within 1.31–1.40, this biosensor ensures high sensitivity and resolution, making it ideal for practical applications such as glucose monitoring and protein interaction analysis.

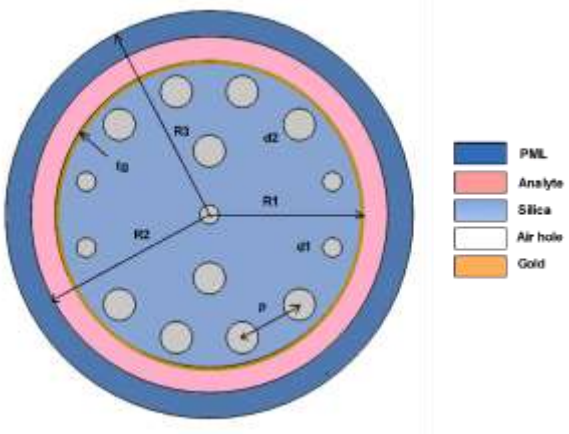

Fig. 2. Proposed Model Geometry

The design of the suggested PCF-SPR biosensor model with a particular configuration and labeled components is shown in Fig. 2.

We have used COMSOL Multiphysics software to design the SPR sensor model. This software uses finite element method (FEM), which is a powerful numerical technique used to solve a wide range of engineering and scientific problems, particularly those involving complex geometries and material properties. This software allows for the modeling of complex physical phenomena, including light propagation within the PCF-SPR structure. Here are the steps that are used for PCF-SPR biosensor design and simulation.

- Define the SPR Model: Establish the geometric structure and specify the material properties involved.

IJARCCE ISSN (O) 2278-1021, ISSN (P) 2319-5940

International Journal of Advanced Research in Computer and Communication Engineering

Impact Factor 8.102 ⁜ Peer-reviewed & Refereed journal ⁜ Vol. 14, Issue 1, January 2025

DOI: 10.17148/IJARCCE.2025.14127

- Set Simulation Parameters: Configure the simulation environment, including the light source, analyte characteristics, and key SPR parameters.
- Execute Simulation: Perform computations to evaluate the propagation of light within the SPR model.
- Analyze Outcomes: Concentrate on critical metrics such as the effective refractive index, confinement loss, and amplitude sensitivity.
- Refine the Design: Modify the geometric and material parameters to enhance performance, aiming for maximum SPR sensitivity and minimal confinement loss.
- Iterative Refinement: Repeat this process to identify the optimal configuration for PCF-SPR sensors, achieving the desired performance criteria.

(a) (b) (c)

Fig. 3. (a) Mesh version (b) SPP mode y-polarized electric field distribution. (b) Core mode y-polarized electric field distribution.

The PCF-SPR biosensor meshes model, the distribution of the y-polarized electric field for the core mode and the SPP mode are shown in Figs. 3(a),(b) and (c), respectively. These visualizations provide insights into the behavior and interaction of electric fields within the proposed PCF-SPR biosensor structure. The Sellmeier equation specifies how to calculate the refractive index of fused silica, which depends on the wavelength of light. The equation is expressed as follows:

$$n^2(\lambda) = 1 + \frac{B_1\lambda^2}{\lambda^2 - C_1} + \frac{B_2\lambda^2}{\lambda^2 - C_2} + \frac{B_3\lambda^2}{\lambda^2 - C_3} \quad (1)$$

Where the Sellmeier constants are B1, B2, B3, C1, C2, and C3. The constants have the following values: C1=0.00467914826, C2=0.0135120631, C3=97.9340025, B1=0.69616300, B2=0.407942600, B3=0.897479400.
CL is assessed through the imaginary part of the N_{eff} [17]. The following equation expresses the relationship:

$$CL\ (dB/cm) = 8.686 \times k_0\, Im(N_{eff}) \times 10^4 \quad (2)$$

Where $k_0 = 2\pi/\lambda$ is the propagation constant, and $Im(N_{eff})$ is the imaginary part of the effective mode refractive index. This equation quantifies the attenuation of light within the sensor due to confinement loss, an essential parameter in assessing the sensor's performance.

AS is an essential metric that measures the sensing capacity of SPR sensors, reflecting the variation in incoming light amplitude. The following equation determines the numerical calculation of amplitude sensitivity [17].

$$AS = -\frac{1}{\alpha(\lambda, n_a)} \frac{\partial \alpha(\lambda, n_a)}{\partial n_a} \quad (3)$$

Here, n_a stands for the refractive index of the analyte, ∂n_a is the difference in refractive indices of two analytes that are next to each other, α (λ, n_a) indicates confinement loss, and $\partial\alpha$ (λ, n_a) indicates variation in confinement loss. This formula measures the impact of variations in the analyte's refractive index on the SPR sensor signal's amplitude.

WS is another essential performance parameter for SPR sensors [17], quantifying the fluctuation of incoming light's wavelength. The definition of wavelength sensitivity involves the following equation:

IJARCCE ISSN (O) 2278-1021, ISSN (P) 2319-5940

International Journal of Advanced Research in Computer and Communication Engineering

Impact Factor 8.102 ⁜ Peer-reviewed & Refereed journal ⁜ Vol. 14, Issue 1, January 2025

DOI: 10.17148/IJARCCE.2025.14127

$$WS = \Delta\lambda_{peak} / \Delta n_a \quad (4)$$

Where $\Delta\lambda_{peak}$ represents the peak wavelength variation, and Δn_a is the variation in refractive index between two adjacent analytes.

The resolution of the sensor plays a vital role in evaluating its detection capabilities. This can be calculated using the equation below, where Δn_a represents a change of 0.01 RIU and $\Delta\lambda_{min}$ is set to 0.1 nm [17].

$$R\ (RIU) = \Delta n_a \times \Delta\lambda_{min} / \Delta\lambda_{peak} \quad (5)$$

Sensor performance also depends on the FOM, often referred to as the signal-to-noise ratio (SNR) [17]. A higher SNR reduces spectral variation, leading to improved design reliability. Enhancing SNR and spectral width improves the sensor's detection limit. The following equation of FOM is:

$$FOM = \frac{S}{FWHM}\frac{nm/RIU}{nm} \quad (6)$$

Where, S denotes the linear slop of the SP wavelength depending on the RI and FWHM denotes the full width at half-maximum.

III. RESULT & DISCUSSION

The computational analysis of the both real and imaginary components of N_{eff} was conducted using COMSOL Multiphysics simulation software to study various propagation characteristics. Figure 4 depicts the phase matching between the SPP mode and the core mode for an analyte refractive index of n_a = 1.36. The figure indicates that the confinement loss initially rises at shorter wavelengths, reaches a peak, and then declines as the wavelength increases. It also illustrates the variation in the effective refractive index with wavelength, showing that N_{eff} decreases as the wavelength becomes longer. Importantly, the real part of N_{eff} for the y-polarized core mode aligns with the real part of N_{eff} for the y-polarized SPP mode at a resonance wavelength of 0.64 µm, known as the phase matching point. At this stage, the confinement loss is at its maximum, and the effective refractive index reaches a value of 1.451.

Figure 5(a) illustrates the confinement loss as a function of wavelength for varying refractive indices (n_a) ranging from 1.31 to 1.4. The confinement loss is measured in dB/cm and shows distinct peaks for each n_a value, shifting toward higher wavelengths as na increases. The maximum confinement loss observed in this case is approximately 179.70 dB/cm at n_a = 1.4. The design parameters used for this analysis are not specified but are critical for influencing the loss characteristics. This analysis highlights the relationship between n_a and wavelength, where increasing n_a leads to higher peak confinement loss values and shifts in resonance, which is significant for applications requiring precise control over waveguide properties. Adjusting the design parameters can optimize these loss and sensitivity characteristics, balancing performance for specific sensor applications.

The relationship between the RI of analytes and AS in the wavelength range of 0.55 µm to 0.85 µm is shown in Figure 5(b). The graphs demonstrate that amplitude sensitivity varies as the wavelength increases, initially rising to a peak value before decreasing. Higher n_a exhibit greater sensitivity to wavelength variations, as evident from the progressive upward shift in the maximum amplitude sensitivity for increasing na ranges. The maximum sensitivity values are observed for refractive index ranges of 1.31–1.32, 1.32–1.33, 1.33–1.34, 1.34–1.35, 1.35–1.36, 1.36–1.37, 1.37–1.38, 1.38-1.39 and 1.39-1.40 with corresponding values of --74.23 RIU^{-1}, -96.93 RIU^{-1}, -133.55 RIU^{-1}, -176.70 RIU^{-1}, -261.94 RIU^{-1}, -388.11 RIU^{-1}, -620.85 RIU^{-1}, -871.86 RIU^{-1} and -1279.38 respectively. Notably, the highest amplitude sensitivity of -1279.38 RIU^{-1} is achieved for the n_a range of 1.39–1.40 at a wavelength of approximately 0.82 µm.

IJARCCE ISSN (O) 2278-1021, ISSN (P) 2319-5940

International Journal of Advanced Research in Computer and Communication Engineering

Impact Factor 8.102 ⁜ Peer-reviewed & Refereed journal ⁜ Vol. 14, Issue 1, January 2025

DOI: 10.17148/IJARCCE.2025.14127

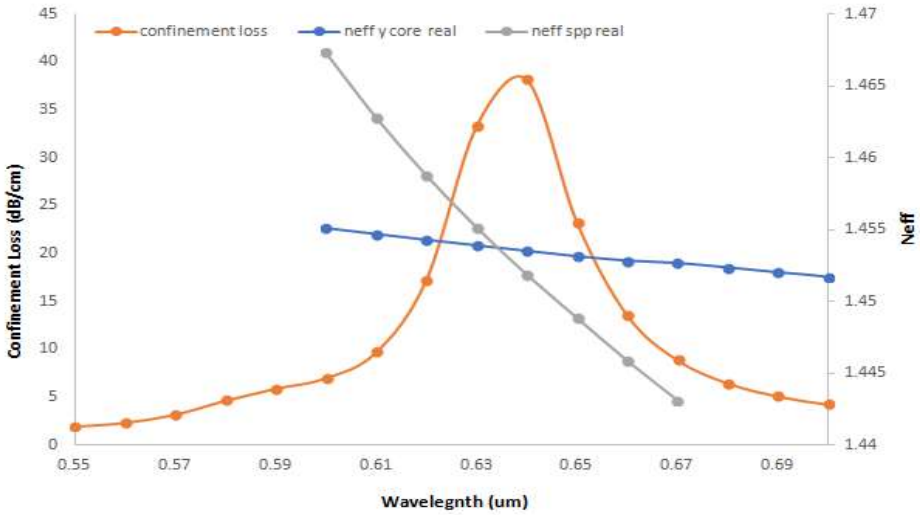

Fig. 4 N_{eff} and confinement loss phase matching between the core and SPP modes.

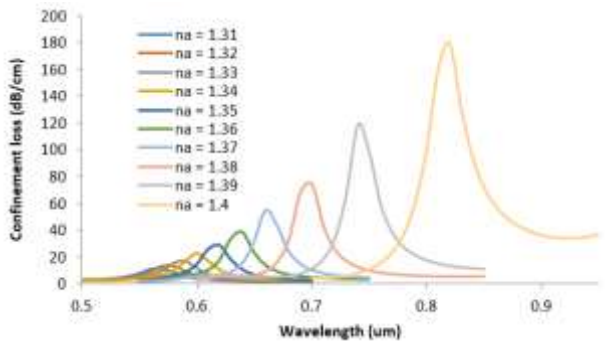

(a)

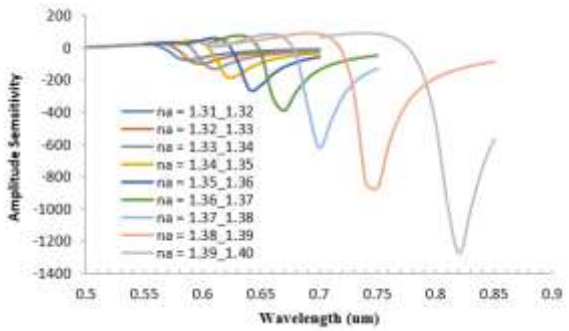

(b)

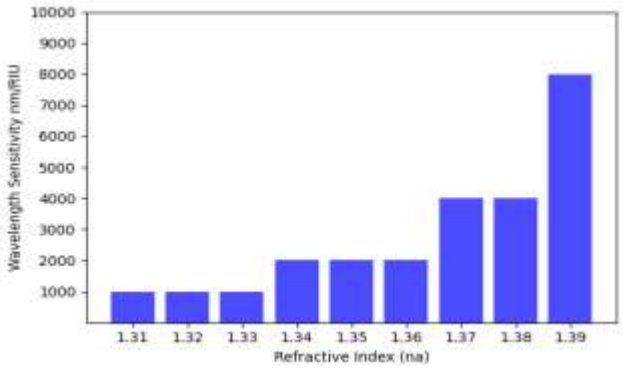

(c)

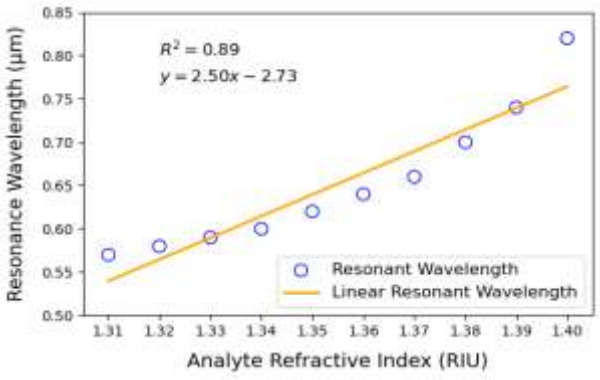

(d)

Figure 5. (a) Confinement loss vs. wavelength for d1=0.6 & d2=1µm, (b) Amplitude sensitivity vs. wavelength for d1=0.6 & d2=1µm (c) Wavelength sensitivity Vs. Refractive Index (d) Linear Correlation between Resonant Wavelength and Analyte Refractive Index

Figure 5(c) illustrates the wavelength sensitivity performance of a novel PCF-based SPR sensor as a function of the RI ranging from 1.31 to 1.39. The sensitivity increases significantly, starting from approximately 1000 nm/RIU at n_a =1.31 and gradually rising up to 9000 nm/RIU at n_a =1.39. Intermediate values show a steady increment: approximately 1000 nm/RIU at n_a = 1.32, 1000 nm/RIU at n_a=1.33, 2000 nm/RIU at n_a=1.34, 3000 nm/RIU at n_a=1.35, 4000 nm/RIU at

DOI: 10.17148/IJARCCE.2025.14127

n_a=1.36, 5000 nm/RIU at n_a=1.37, and 5000 nm/RIU at n_a=1.38. This enhancement demonstrates the sensor's capability to detect minor RI index variations with high precision, making it highly suitable for advanced biochemical and environmental sensing applications.

Figure 5(d) illustrates the relationship between the analyte RI and the resonant wavelength as measured by the proposed PCF-SPR sensor. The blue circles represent experimental data points correlating the analyte RI (x-axis) with the resonant wavelength (y-axis), while the orange line represents the optimal linear fit, expressed by the equation $y = 2.50x - 2.73$. Here, y is the resonant wavelength, and x is the analyte . The slope 2.50 quantifies the rate of change in the resonant wavelength per unit change in RI, demonstrating the sensor's sensitivity to refractive index variations. The coefficient of determination ($R^2 = 0.89$) indicates that 89% of the variation in the resonant wavelength is explained by the linear model, highlighting a strong correlation. The data demonstrates a direct and proportional relationship, where increases in the analyte RI correspond to upward shifts in the resonant wavelength. This predictable and consistent relationship confirms the PCF-SPR sensor's capability to accurately estimate unknown refractive indices, making it highly suitable for detecting and quantifying analytes across a broad sensing range.

The proposed model performance analysis is shown in Table 2. A steady trend is observed in terms of confinement loss, peak wavelength (λ_{peak}), and AS over a wide range of n_a. As n_a increases from 1.31 to 1.40, the confinement loss increases significantly, ranging from 11.04 dB/cm to 179.71 dB/cm. The λ_{peak} shifts progressively from 570 nm to 820 nm. The AS also shows a marked increase in magnitude, indicating enhanced sensitivity with increasing n_a. Additionally, the R, WS, and FOM vary based on the analyte index, demonstrating the sensor's adaptability across different refractive indices. The highest FOM is observed at n_a = 1.39, with a value of 250.00 RIU^{-1}, corresponding to the highest WS (8000 nm/RIU) and the lowest resolution (1.25×10^{-5} RIU).

TABLE II THE PROPERTIES OF THE PROPOSED SPRBIOSENSOR WITH DIFFERENT ANALYTES VALUES

n_a	peak wl (μm)	peak CL (dB/cm)	peak wl (nm)	$\Delta\lambda_{peak}$	WS (nm/RIU)	Resolution (R) (RIU)	FOM (RIU^{-1})
1.31	0.57	11.0389859	570	10	1000	1.00×10^{-4}	22.22
1.32	0.58	13.36585646	580	10	1000	1.00×10^{-4}	22.22
1.33	0.59	17.10140283	590	10	1000	1.00×10^{-4}	25.00
1.34	0.6	22.7002827	600	20	2000	5.00×10^{-5}	57.14
1.35	0.62	28.32324068	620	20	2000	5.00×10^{-5}	57.14
1.36	0.64	38.18586946	640	20	2000	5.00×10^{-5}	64.52
1.37	0.66	54.67106317	660	40	4000	2.50×10^{-5}	100.00
1.38	0.7	73.92914186	700	40	4000	2.50×10^{-5}	129.03
1.39	0.74	118.4930703	740	80	8000	1.25×10^{-5}	250.00
1.4	0.82	179.7092621	820	-	-	-	-

TABLE III COMPARATIVE STUDIES OF PERFORMANCE ANALYSIS WITH PREVIOUS WORK

References	n_a	Maximum WS (nm/RIU)	Maximum AS (RIU^{-1})	R (RIU)	FOM(RIU^{-1})
[12] (2020)	1.21–1.40	5000	1277.47	2.0×10^{-5}	*
[18] (2021)	1.32-1.41	4200	450	2.3×10^{-5}	*
[19] (2022)	1.33–1.40	6700	2146	1.49×10^{-5}	*
[20] (2023)	1.33-1.40	7000	593.61	1.43×10^{-5}	*
[21](2024)	1.31-1.39	4000	5607.58	*	*
[22](2024)	1.28-1.44	1000	98.422	0.001	*
[23](2024)	1.36-1.38	7500	800	1.54×10−6	73

DOI: 10.17148/IJARCCE.2025.14127

[24](2024)	1.33-1.39	7142.86	4220.99	3.33×10−5	*
[25](2025)	1.373 – 1.402	6250	673.86	2.1 × 10−5	*
proposed	1.31-1.40	8000	-1279.38	1.25×10^{-5}	250

Table 3 compares the performance of different models in biosensing applications based on key design parameters. Reference [12] investigated a refractive index range of 1.21–1.40, achieving a maximum shift WS of 5000 nm/RIU, AS of 1277.47 RIU^{-1}, and R of 2.0×10^{-5} RIU. Reference [18] explored 1.32–1.41, reporting a WS of 4200 nm/RIU, AS of 450 RIU^{-1}, and R of 2.3×10^{-5} RIU. Reference [19] achieved a WS of 6700 nm/RIU, AS of 2146 RIU^{-1}, and R of 1.49×10^{-5} RIU for a range of 1.33–1.40. Reference [20] demonstrated a WS of 7000 nm/RIU, AS of 593.61 RIU^{-1}, and R of 1.43×10^{-5} RIU in the same refractive index range. Reference [21] focused on 1.31–1.39, achieving a WS of 4000 nm/RIU, an exceptional AS of 5607.58 RIU^{-1}, but did not specify resolution or FOM. Reference [22] examined a range of 1.30–1.38, achieving a WS of 4800 nm/RIU, AS of 3900 RIU^{-1}, and a resolution of 1.35×10^{-5} RIU. Reference [22] demonstrated precision with a high resolution of 0.001 RIU across a wide refractive index range of 1.28 to 1.44, despite a lower WS of 1000 nm/RIU. Reference [23] achieved the highest WS of 7500 nm/RIU within a narrower range of 1.36 to 1.38, paired with an exceptionally fine resolution of 1.54×10^{-6} RIU and a FOM of 73 RIU^{-1}, indicating a highly sensitive model. Reference [24] offered strong sensitivity and specificity with a WS of 7142.86 nm/RIU and an AS of 4220.99 RIU^{-1}, alongside the best resolution of 3.33×10^{-5} RIU. Finally, reference [25] extended capabilities to a broader index range of 1.373 to 1.402 with a WS of 6250 nm/RIU and an AS of 673.86 RIU^{-1}, showcasing robust performance.

In comparison, the proposed model demonstrated superior performance in the RI range of 1.31–1.40. It achieved a maximum WS of 8000 nm/RIU, SA of -1279.38 1/RIU, a competitive R of 1.25×10^{-5} RIU, and an impressive FOM of 250 RIU^{-1}, outperforming most previous studies. These results underline the proposed model's strong spectral sensitivity, with its maximum WS being the highest reported in this range. Although the SA is negative, it represents a unique feature, and the high FOM and precise R further emphasize its effectiveness, making the model highly competitive for high-sensitivity and high-resolution practical biosensing applications. The proposed model demonstrated superior performance in detecting analytes with refractive indices in the range of 1.31–1.40, making it highly suitable for applications such as glucose monitoring and protein interaction analysis in medical diagnostics.

IV. CONCLUSION

This research highlights the development of a high-performance dual-core, gold-coated PCF-SPR biosensor that covered a broad RI range of 1.31–1.40. The sensor exhibited outstanding performance, achieving a maximum wavelength sensitivity of 8000 nm/RIU, an amplitude sensitivity of -1279.38 1/RIU, and an improved resolution of 1.25×10^{-5} RIU, making it highly effective for biological and chemical sensing applications. With a FOM of 250 RIU^{-1}, it also shows a high signal-to-noise ratio, making it highly efficient in detecting subtle molecular interactions. The excellent sensitivity and resolution of the biosensor enable precise detection of small refractive index changes, showcasing its potential for high-accuracy biosensing in fields like medical diagnostics, glucose monitoring, and protein interaction analysis. Future work will focus on applying machine learning techniques to optimize sensor performance, such as real-time data analysis, prediction of molecular interactions, and improving the detection of complex analytes.

REFERENCES

[1]. Li, Hongwei, et al. "Prediction of the optical properties in photonic crystal fiber using support vector machine based on radial basis functions." Optik 275 (2023): 170603.

[2]. Islam, Mohammad Rakibul, et al. "Design and analysis of birefringent SPR based PCF biosensor with ultra-high sensitivity and low loss." Optik 221 (2020): 165311.

[3]. Kumar, Amit, Pankaj Verma, and Poonam Jindal. "Surface plasmon resonance sensor based on MXene coated PCF for detecting the cancer cells with machine learning approach." Microelectronic Engineering 267 (2023): 111897.

[4]. Robinson, Grenville. "The commercial development of planar optical biosensors." Sensors and Actuators B: Chemical 29.1-3 (1995): 31-36.

[5]. Hossain, M. M., & Maniruzzaman, M. (2015, June). Study of confinement loss in photonic crystal fiber. In International Conference on Materials, Electronics & Information Engineering.

[6]. Hossain, Md Mahbub, and Md Maniruzzaman. "Analysis of dispersion and confinement loss in photonic crystal fiber." 2014 International Conference on Electrical Engineering and Information & Communication Technology. IEEE, 2014.

International Journal of Advanced Research in Computer and Communication Engineering

Impact Factor 8.102 ⁜ Peer-reviewed & Refereed journal ⁜ Vol. 14, Issue 1, January 2025

DOI: 10.17148/IJARCCE.2025.14127

[7]. Rifat, Ahmmed A., et al. "Photonic crystal fiber-based surface plasmon resonance sensor with selective analyte channels and graphene-silver deposited core." Sensors 15.5 (2015): 11499-11510.

[8]. Otupiri, R., Emmanuel K. Akowuah, and Shyqyri Haxha. "Multi-channel SPR biosensor based on PCF for multi-analyte sensing applications." Optics Express 23.12 (2015): 15716-15727.

[9]. Zakaria, Rozalina, et al. "Fabrication and simulation studies on D-shaped optical fiber sensor via surface plasmon resonance." Journal of Modern Optics 64.14 (2017): 1443-1449.

[10]. Xue, Jianrong, et al. "Polarization filter characters of the gold-coated and the liquid-filled photonic crystal fiber based on surface plasmon resonance." Optics Express 21.11 (2013): 13733-13740.

[11]. Lu, Ying, et al. "Surface plasmon resonance sensor based on hollow-core PCFs filled with silver nanowires." Electronics Letters 51.21 (2015): 1675-1677.

[12]. Roni, Tanvir Alam, Rifat Hassan, and Mohammad Faisal. "Dual-side polished SPR biosensor with wide sensing range." 2020 11th.

[13]. Chen, Nan, et al. "Highly sensitive plasmonic sensor based International Conference on Electrical and Computer Engineering (ICECE). IEEE, 2020.

[14]. Roh, Sookyoung, Taerin Chung, and Byoungho Lee. "Overview of the characteristics of micro-and nano-structured surface plasmon resonance sensors." Sensors 11.2 (2011): 1565-1588.

[15]. Dash, Jitendra Narayan, and Rajan Jha. "Highly sensitive side-polished birefringent PCF-based SPR sensor in near IR." Plasmonics 11 (2016): 1505-1509

[16]. Dash, Jitendra Narayan, and Rajan Jha. "Graphene-based birefringent photonic crystal fiber sensor using surface plasmon resonance." IEEE Photonics Technology Letters 26.11 (2014): 1092-1095.

[17]. Sakib, Md Nazmus, et al. "High-performance dual-core D-shape PCF-SPR sensor modeling employing gold coat." Results in Physics 15 (2019): 102788.

[18]. Yang, Hongyan, et al. "Highly sensitive graphene-Au coated plasmon resonance PCF sensor." Sensors 21.3 (2021): 818.

[19]. Jabir, Jamal Nasir, and Nabeel Abbas Areebi. "High sensitively of double-core surface plasmon resonance biosensor based on photonic crystal fiber." Optical and Quantum Electronics 54.10 (2022): 626.

[20]. Islam, Nazrul, et al. "Highly sensitive open channel based PCF-SPR sensor for analyte refractive index sensing." Results in Physics 46 (2023): 106266

[21]. Khatun, M. R., and Mithila Akter Mim. "Analysis of Highly Sensitive Simple Designed PCF-Based SPR Biosensor." 2024 6th International Conference on Electrical Engineering and Information & Communication Technology (ICEEICT). IEEE, 2024.

[22]. Guedri-Knani, Lamia, Sameh Kaziz, and Cherif Dridi. "Optimizing and Predicting Performance of Dual-Side Polished SPR Photonic Crystal Fiber using MLR and ANN Models." Plasmonics (2024): 1-12. https://doi.org/10.1007/s11468-024-02534-8

[23]. Emon, Wahiduzzaman, et al. "Photonic crystal fiber-based spr biosensor coated with ag-tio2 and au-tio2 for the detection of skin cancer: a comparison." Optical and Quantum Electronics 56.8 (2024): 1322. https://doi.org/10.1007/s11082-024-07250-5

[24]. Ibrahimi, Khalid Mohd, R. Kumar, and Writtick Pakhira. "Early detection of cancer cells using high-sensitivity dual-side polished photonic crystal fiber biosensors based on surface plasmon resonance." Optical and Quantum Electronics 56.5 (2024): 888. https://doi.org/10.1007/s11082-024-06782-0

[25]. Yasli, Ahmet, and Huseyin Ademgil. "Simultaneous detection of ague stages by using a multi-inner channel photonic crystal fiber based surface plasmon resonance sensor." Journal of Computational Electronics 24.1 (2025): 1-15. https://doi.org/10.1007/s10825-024-02260-8